

Article

Mechanical Performance of Concrete Segment Lining Structure of Shield Tunneling in Different Strata

Hui Hu ^{1,*}, Tao Xue ², Jianjun Li ³, Peisi Liu ⁴, Bo Wang ¹ and Yun Liu ¹

¹ Key Laboratory of Transportation Tunnel Engineering, Ministry of Education, Southwest Jiaotong University, Chengdu 610031, China; wangbo36996321@126.com (B.W.); yunliu99@my.swjtu.edu.cn (Y.L.)

² China Communications Construction Company Limited, Beijing 100088, China; taoxue_cccc@163.com

³ China Railway Materials Group Xinjiang Co., Ltd., Urumqi 830011, China; lijianjun2222023@163.com

⁴ China Railway Eryuan Engineering Group Co., Ltd., Chengdu 610031, China; peisi_l@outlook.com

* Correspondence: huihu@home.swjtu.edu.cn; Tel.: +86-028-87634386

Abstract: There are many problems in the development of urban space in China. Among them, urban tunnels generally pass through many sections with very complicated geological conditions, and the construction will encounter great difficulties, so the mechanical behavior of shield segments in different complex strata is worth discussing. In this paper, the axial force, bending moment and pore water pressure of shield tunnel segments in the soft and hard uneven stratum, clay stratum and fully weathered granite stratum of overlying buildings are studied by establishing a rectangular element mechanical model based on the field test method. The analysis shows that the mechanical properties of shield tunnels in different strata are quite different, but their mechanical properties change stages are the same. The earth pressure on the left and right sides of the test ring is asymmetric in the soft and hard uneven stratum, and the vault pressure is much greater than the vault bottom pressure. The distribution of earth pressure in each position of the segment ring in clay stratum is relatively balanced, and the earth pressure on both sides is relatively small; in the fully weathered granite layer of the overlying building, the segment ring of the test ring is subjected to greater additional stress, and the internal force of the segment is much greater than that without the overlying building. Exploring the similarities and differences of segment stress in these three complex strata can provide an important basis for the design and construction of shield segments in complex strata.



Citation: Hu, H.; Xue, T.; Li, J.; Liu, P.; Wang, B.; Liu, Y. Mechanical Performance of Concrete Segment Lining Structure of Shield Tunneling in Different Strata. *Buildings* **2023**, *13*, 3118. <https://doi.org/10.3390/buildings13123118>

Academic Editor: Chiara Bedon

Received: 16 November 2023

Revised: 7 December 2023

Accepted: 14 December 2023

Published: 15 December 2023



Copyright: © 2023 by the authors. Licensee MDPI, Basel, Switzerland. This article is an open access article distributed under the terms and conditions of the Creative Commons Attribution (CC BY) license (<https://creativecommons.org/licenses/by/4.0/>).

Keywords: tunnel; shield segment; soft and hard uneven strata; clay formation; adjacent pile foundation; water pressure

1. Introduction

With the development of urbanization in China, the utilization rate of urban land can not fully meet the needs. Underground space, as an important national natural resource, can provide large-scale and stable space support, and the existence of low-carbon technology now has a great environmental protection effect [1]. The development direction of urban space is to change from horizontal direction to vertical direction, which will require many underground structures [2–5]. The underground rapid transit system has become an important means of transportation, and the subway has become the main basic transportation facility to alleviate the ground traffic saturation in many cities. By the end of 2021, the area of Chinese mainland participating in rail transit construction exceeded 9000 km [6].

Although the development of urban underground space has detailed planning and arrangement before construction, in the long run, it still has some unpredictability. When the construction is carried out in a highly supervised and controlled way, compared with the drilling and blasting method [7–9], the shield method has become the preferred construction scheme because of its advantages of less interference to the stratum, high speed and high efficiency [10–14]. Although the shield tunnel has many advantages mentioned above, and

the construction technology has made great progress over the years, due to the defects of geological conditions and construction technology, the advancement of the shield tunnel will inevitably cause disturbance, which will change the stress state of the soil and cause the ground displacement [15–18], and the disturbance to the ground will cause the stress change of the shield segment and the damage of the shield tunnel lining [19,20].

At present, the mechanical analysis of the segment structure of the shield tunnel is mainly aimed at the stress analysis after tunnel construction is completed, but there are many factors affecting the stress of the segment during construction, and there are few studies at this stage [21–24]. Most of them are mainly used for the stress analysis of segment structure in normal use stage, and the influence of various factors on segment stress in construction stage is basically ignored [25]. A large number of shield engineering practices show that it will take a period of time from the segment assembly into a ring to the final solidification of slurry and the close adhesion of surrounding rock. In this process, the stress on the segment is very complicated, including jack pressure, longitudinal bending and torsion [26,27], surrounding rock and grouting pressure, and unfavorable internal force caused by segment assembly, which leads to various forms of damage of the lining segment. From practical experience, segment cracking mostly occurs in the construction stage, which leads to water leakage, which can not guarantee its quality and directly affect the safe use and durability of the tunnel [28]. At present, many studies at home and abroad are aimed at several design models [29–33]. Zhu et al. [30,31], in studying the new design model, the beam-joint discontinuity model, use the field measured value of segment internal force to determine the distribution mode and magnitude of pressure load acting on the lining structure. The consistent relationship between the straight beam-spring model and the curved beam-spring model is also discussed. Chen et al. [32] compared the measured simulation results with the design values according to the field test results of the shield segment of a subway tunnel, and studied the working characteristics of the shield segment under different working conditions. Hu et al. [33] studied the connection characteristics between segment lining structures of the shield tunnel and the interaction between the soil layer and the segment lining structure, and put forward a flat shell-elastic hinge-foundation system model of the segment lining structure of the shield tunnel, which can solve the three-dimensional stress analysis of the segment lining structure of the shield tunnel. Kong et al. [34] set up a model test device to carry out a shield unbalanced load test during tunnel excavation. The model test of shield tunneling in the upper soft and lower hard stratum is carried out to verify the function of the developed test system. Zou et al. [35] used a large model test platform to test this synchronization technology. The theoretical external load is applied to the shield machine to simulate the construction process of a single circle straight line. The effectiveness of the redistribution principle for thrust loss caused by the withdrawal of the cylinder located in the segment manufacturing area is discussed. Sazid et al. [36] established the three-dimensional model of the tunnel and its surrounding rock by the finite element method. The displacement vector before and after tunnel excavation, the stress of the model and its corresponding strain distribution are analyzed. Verma et al. [37] studied the geotechnical characteristics along the 1800 m-long tunnel in Bansagar. The stress–strain distribution of tunnel excavation and the support system is also numerically analyzed. The Mohr–Coulomb elastic-plastic constitutive model is used for a series of finite element analysis. The stability of the tunnel is analyzed and the stress mode is discussed. Relying on the shield construction of the Shenzhen urban rail transit Line 5 tunnel, based on the test method, it is difficult to truly reflect the actual stress of the segment lining in the project by using a simple and single calculation theory, while the field test of the shield segment can accurately reflect the real stress of the segment under various conditions. We can find out the actual stress state of the segment in uneven soft and hard stratum and clay stratum, and the influence of building pile foundation close to the shield tunnel on the internal force of the segment, which provides the basis for theoretical analysis of tunnel structure stress and optimal design of the segment [23].

2. Project Overview

Shenzhen Metro Line 5 is a backbone line of Shenzhen that connects north and south, connects west and expands east, and expands external transportation in the inland hinterland, with a total length of 40.001 km. Metro Line 5 plays a prominent and irreplaceable role in building the framework of the near to medium term rail network and maximizing the benefits of the rail network. It is an important and special backbone line in the Shenzhen rail transit network, as shown in Figure 1.



Figure 1. Route map and three sections of Shenzhen Metro Line 5.

Shenzhen Metro Line 5 runs east–west as a whole, starting from Qianwan Bay, Nanshan District, passing through Nanshan District, Bao’an District, Longgang District and Luohu District in sequence, and ending at Huangbeiling. The shield section is a circular tunnel between two parallel separate single-line circular tunnels. The designed outer diameter of the segment is 6 m, the inner diameter is 5.4 m, the limit is 5.2 m, the thickness of the segment is 30 cm and the width is 1.5 m. The segment number is 6, which is the “3 + 2 + 1” segmentation mode. Each ring segment is composed of three standard blocks, two adjacent blocks and one capping block. The segment wedge is 38 mm. Staggered stitching is used. The segment concrete grade is C50, and the impermeability grade is not less than S10. The minimum curve radius of the tunnel is $R = 400$ m. After the shield is launched, the longitudinal slope of the line is laid out in a “V” shape, with a maximum longitudinal slope of 28%. The minimum distance between the left and right lines of the interval is 8.7 m, and the maximum distance is 32.3 m. The burial depth of the tunnel structure vault is 9.8 m to 32.4 m, and its burial depth is below the groundwater level.

The shield tunnel of this project will pass through many areas with very complex environmental and geological conditions, and the construction will encounter great difficulties. This article mainly discusses three adverse geological conditions: uneven soft and hard strata, clay strata and adjacent pile foundations. The section from Yijing Road to Huangbeiling in the first bidding section passes through five residential buildings in Jingbei Garden Community and many underground pipelines, including the Xinxiu Pedestrian Bridge, with the minimum distance between the tunnel and the bridge piles being 3.27 m. The shield tunnel in this section traverses unevenly soft and hard strata. The upper part of the tunnel in the entire section is mostly composed of gravel, sand and clay layers. Within the tunnel body, there are intrusions of Sinian fully to slightly weathered mixed rock and Jurassic tuff. The maximum intrusion height is 6 m. The shield tunnel in the second bid section will pass through gravelly clay soil, fully-strongly weathered granite, and partially through medium-lightly weathered rock formations. The phenomenon of uneven softness and hardness in the same section of the stratum traversed by the shield tunnel in this section will be particularly prominent, and the frequency of changes will be high. The

uniaxial strength of hard rock is as high as 200 MPa, making construction difficult and technically demanding.

3. Test Preparation, Component Installation and Data Collection

3.1. Selection of Test Sections

Combined with the hydrogeological characteristics and construction progress of this project, three sections of the shield section of Shenzhen Metro Line 5 are selected, as shown in Figure 1.

Section I is the 465th ring (shield standard ring) at DK38 + 654 on the left line of the section between Yijing Road station and Huangbeiling station. The depth of the tunnel in this section is 17 m, and the groundwater level is 3.5 m above the ground. The tunnel is located in three strata with different hardness: strongly weathered tuffaceous sandstone, weathered tuffaceous sandstone and slightly weathered tuffaceous sandstone. The geological conditions are complex and are typical: soft and hard uneven strata.

Section II is the 375th ring (shield standard ring) at DK5 + 020 on the left line of the section between Fanshen station and Lingzhi station. The vault depth of the test section is 15.5 m, and the underground water level is 3.5 m. The tunnel is located in a gravelly clay soil layer, which is a typical clay formation.

Section III is the 213th ring (special shield reinforced standard ring) at DK4 + 521 on the right line of the section between Fanshen station and Lingzhi station. The burial depth of this section is 20.5 m, and the groundwater level is 3.2 m. The tunnel is located in three strata with different hardnesses: gravelly clay soil, fully weathered granite and strongly weathered granite. The geological conditions are complex. The upper surface of the test ring segment is covered with Bihaihuayuan Community.

3.2. Installation of Test Components

The internal force testing instrument of the segment uses the TFL-S-NM 15 vibrating wire concrete micro-strain gauge (Tianjin Weikende Measurement and Control Equipment Technology Co., Ltd. Tianjin, China) with a measuring range of $+1500 \sim -1500 \mu\epsilon$; the steel bar axial force test uses the TFL-S-GJ 20 vibrating wire steel bar gauge (Nanjing Genan Industry Co., Ltd. Nanjing, China) with a measuring range of 500 MPa. Reinforcement gauges and concrete strain gauges are pre-fixed to the prefabricated steel cage before the segment concrete is cast on site. After the position of the test components is fixed, all the special test cables are introduced into the special wiring holes, and the outlet pipes are sealed with tape before the shield tunnel segment concrete is poured. There are 10 earth pressure measuring points on each section, that is, there are two segments A1, A2, A3, B and C, and the central angle between each two measuring points is 36° . Because measuring earth pressure requires contact with surrounding rock, the measuring points should be arranged on the outer surface of the segment. Because the shield segment is 30 cm thick, the stress on the upper surface and the lower surface of the segment is quite different, so each section needs to be equipped with 20 concrete strain gauges and reinforcement gauges, that is, 10 on the upper surface and 10 on the lower surface. The layout of test components, steel bar gauges and concrete strain gauges after installation are shown in Figure 2.

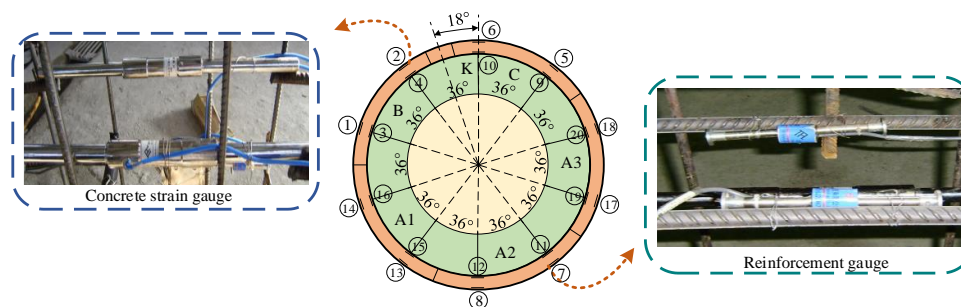


Figure 2. Layout of testing element.

3.3. Test Segment Data Collection

The sensing instruments used in the test are all vibrating wire sensors, and the test data collection uses the TFL-F-BX01 vibrating wire recorder (Beijing Shengkerui Instrument Co., Ltd. Beijing, China) for automatic or manual frequency collection. Figure 3 shows the black cables distributed around the pipe section, showing the wiring of the test components and the data collection process during the field test.



Figure 3. Trend of testing element and data collection.

After the test segments are assembled, the actual stress state measured through tests is very complicated. In order to facilitate understanding and calculation, two assumptions are made without affecting the calculation results:

- (1) It is assumed that the circumferential joints of the segment have no influence on the force of the segment, and the force between the segments is continuous;
- (2) Take a calculation unit in the circumferential direction of the segment and simplify the arc segment into a rectangular unit.

Establish a rectangular unit mechanical model, as shown in Figure 4. Calculate the circumferential force of the segment as an eccentric compression member, in which the main steel and concrete bear the pressure together. The circumferential length of the segment is 1 m as the calculation unit. N_1 and N_2 are the axial force of the single steel bar inside and outside the segment, N_c is the resultant force of the circumferential concrete pressure on the section, M is the circumferential section bending moment, a' is the thickness of the steel protective layer, and the protective layer thickness of the upper and lower steel bars is equal, both 35 mm. According to the measured results, we can know the concrete stress values σ_{c1} and σ_{c2} inside and outside the section, the axial forces N_1 and N_2 inside and outside the steel bar, the longitudinal cross-sectional area of the segment A and the axial force of the longitudinal section of the segment is determined by the axial force on the concrete. N_c consists of the axial force N_s on the steel bar, and the cross-sectional bending moment consists of the bending moment M_c on the concrete and the bending moment M_s on the steel bar. According to the static equilibrium conditions and the material mechanics pressure-bending combination calculation formula, the available force balance equation is as follows [38]:

$$N = N_c + N_s = \left(\frac{\sigma_{c1} + \sigma_{c2}}{2} \right) A + n(N_1 + N_2) \quad (1)$$

$$M = M_c + M_s = n(N_2 - N_1) \left(\frac{h}{2} - a' \right) + \frac{1}{12} (\sigma_{c2} - \sigma_{c1}) Ah \quad (2)$$

$$A = bh \quad (3)$$

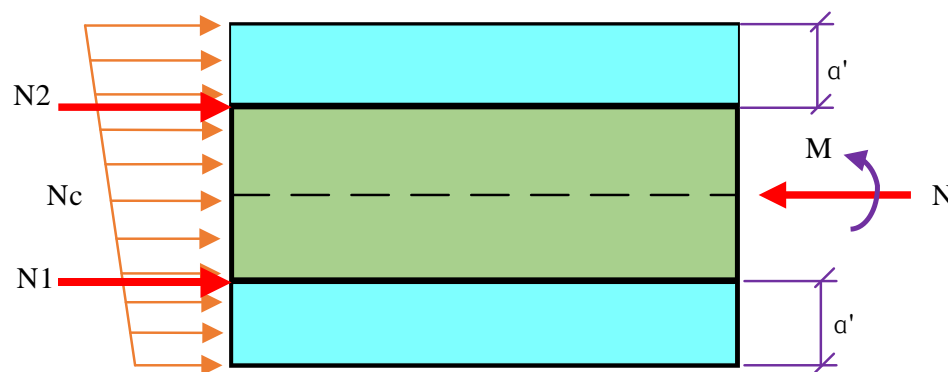


Figure 4. Mechanical model of segment rectangular element.

In the formula, b , h —the width and thickness of the section; (the width of a single segment is 1.5 m for b and 0.3 m for h), n —the number of steel bars inside and outside the segment, both of which are 12.

4. Test Results and Analysis

When the test ring was first assembled, since it was protected by the shield tail and did not come into contact with the surrounding soil and the synchronization slurry, the earth pressure box was not affected by the earth pressure until the test ring came out of the shield tail, that is, from the third position after assembly. Starting from ring 3, the outer surface of the test ring is in contact with the synchronized slurry, and the earth pressure box begins to be affected by pressure.

4.1. Soft and Hard Uneven Formation

4.1.1. Distribution Law of Soil Pressure on Pipe Segments

It can be seen from the change curve of earth pressure with construction in Figure 5 that when the test ring just came out of the shield tail, the earth pressure at each measuring point basically reached the maximum value. This is because the test ring just left the support of the shield machine shell. During protection, the overlying soil pressure begins to act on the test ring. At the same time, the outer surface of the test ring is also affected by the simultaneous grouting pressure of the shield tail and the scraping of the shield tail brush. At that time, the earth pressure value is the partial overlying soil pressure and grouting pressure, the result of superposition. Since the initial setting time of the slurry is only about 6 h, according to the construction progress of eight rings/day, when the test ring is the second ring after coming out of the shield tail, the slurry on the outer circumference of the test ring begins to solidify, and its strength and stiffness gradually increase. At that time, the influence of the rear grouting pressure on the earth pressure at each measuring point is becoming smaller and smaller, while the unreleased overlying earth pressure acts on the test ring through the solidified slurry layer. The earth pressure value at this time is relative; the test ring should be small when it just comes out of the tail of the shield. As the construction continues, the earth pressure value still has a decreasing trend. This is because the grout reaches 70% strength at about 15 rings, and the grouting pressure basically has no effect on the earth pressure. At the same time, the deformation of the overlying soil layer gradually converges; the earth pressure transmitted from the formation pressure to the test ring through the slurry consolidation layer remains basically unchanged. The stabilized earth pressure values at each measuring point are less than the theoretically calculated values. The stabilized soil pressure is shown in Figure 6.

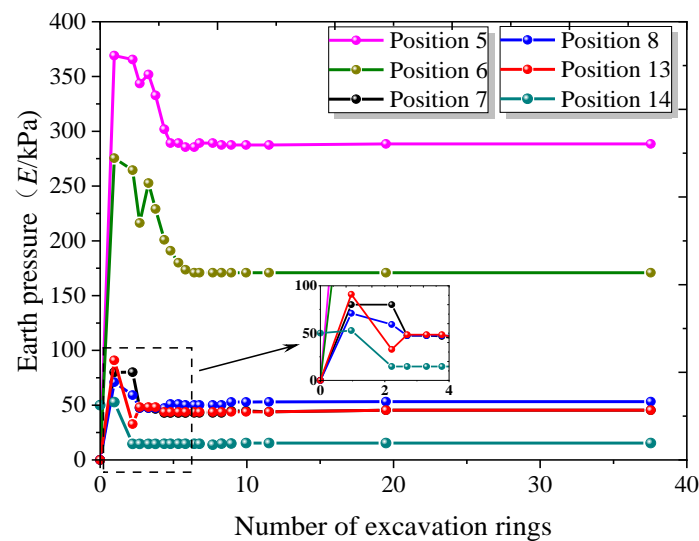


Figure 5. Earth pressure (E) with the construction changes.

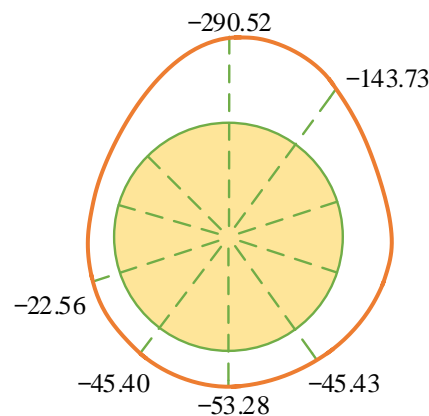


Figure 6. Arrangement of earth pressure (E) after stable (kPa).

Due to the different softness and hardness of the soil, its lateral pressure coefficient and ability to resist deformation are different, resulting in the soil pressure on the left and right sides of the test ring being asymmetrical, and the pressure at the top of the vault is much greater than the pressure at the bottom of the vault. During shield tunneling in strata with uneven softness and hardness, when the test ring segment comes out of the 20 rings of the shield tail, it will take about 4 to 5 days for the stratum to reach a stable state. This is because the geological conditions of unevenly soft and hard strata are relatively complex, there is soil layering, and the mechanical properties of various soils are quite different. During shield tunneling construction, the soil takes a relatively long time to complete the settlement deformation of the strata, the process of forming an arch balance effect and finally reaching a stable state.

4.1.2. Distribution Rules of Internal Forces in Segments

By substituting the collected frequency value of the steel bar meter into the calculation formula of the steel bar axial force and concrete strain, the axial force of the steel bar at each measuring point and the strain of the concrete at each measuring point can be obtained, as well as the change curve of the steel bar axial force with construction and the change curve of concrete strain with construction, as shown in Figures 7 and 8, respectively.

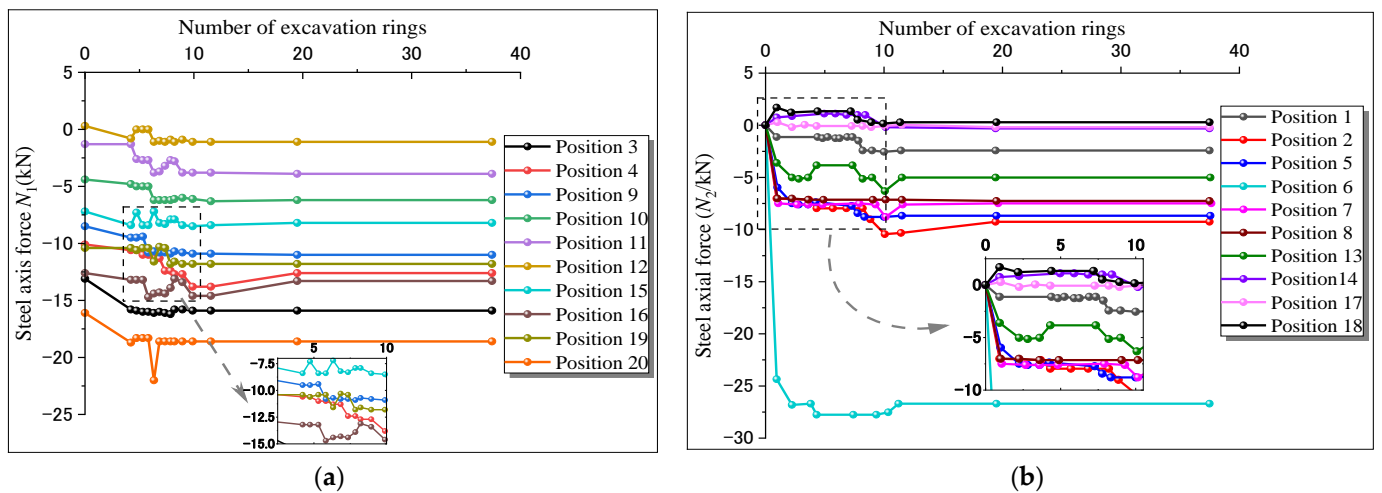


Figure 7. Change curve of steel bar axial force at each measuring point with construction: (a) Axial force (N_1) change curve of inner steel bar. (b) Axial force (N_2) change curve of outer steel bars.

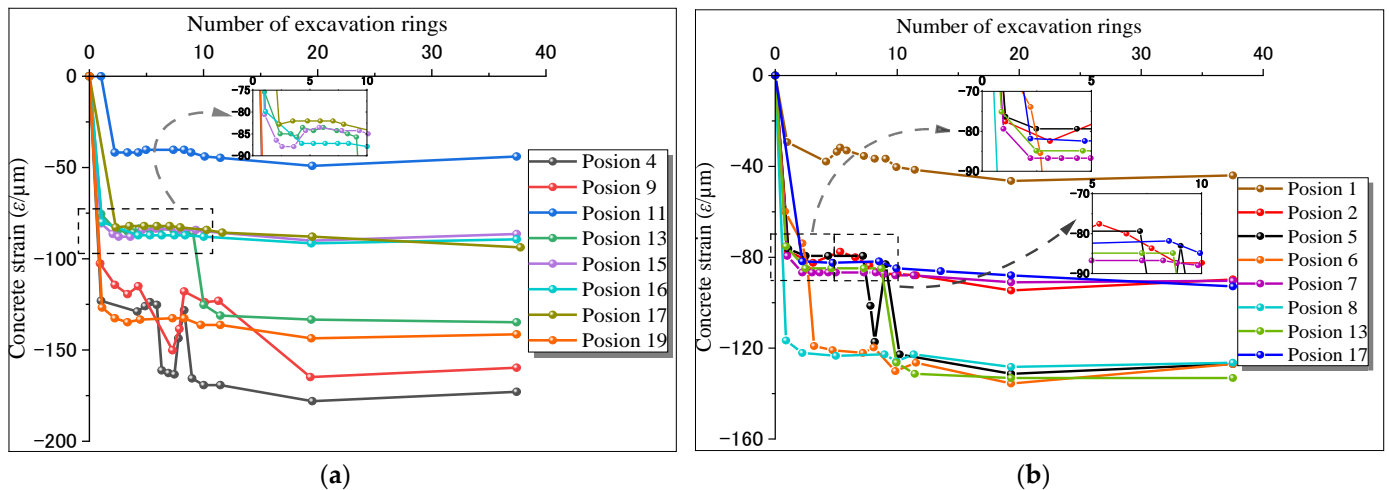


Figure 8. Change curve of concrete strain (ϵ) at each measuring point with construction: (a) Inside concrete strain (ϵ) change curve. (b) External concrete strain (ϵ) change curve.

Assuming that the actual measured axial force of a single steel bar represents the stress level of the circumferential stress-bearing reinforcement of a single-width segment in this section, and there are 12 circumferential stress-bearing reinforcements on the inner and outer sides of the segment, then the data are substituted into Equations (1)–(3), and the axial force and bending moment borne by the newly assembled steel bars of the test ring segment can be obtained. The bending moment is positive when the outer side is tensile, and the axial force is positive when the tensile force is.

Assuming that the concrete strain (ϵ) at the measuring point represents the circumferential inner or outer concrete strain level of the single-width segment of this section, then after substituting the data into Equations (1)–(3), we can obtain the axial force (N) and bending moment; the outer side of the bending moment is positive in tension, and the axial force in tension is positive.

Based on the above-required internal forces of the steel bars and the internal forces of the concrete in each stage of the test ring, superimpose them to obtain the internal force distribution of the test ring segments in the three stages of just assembling, coming out of the shield tail and reaching stability, as shown in Figure 9.

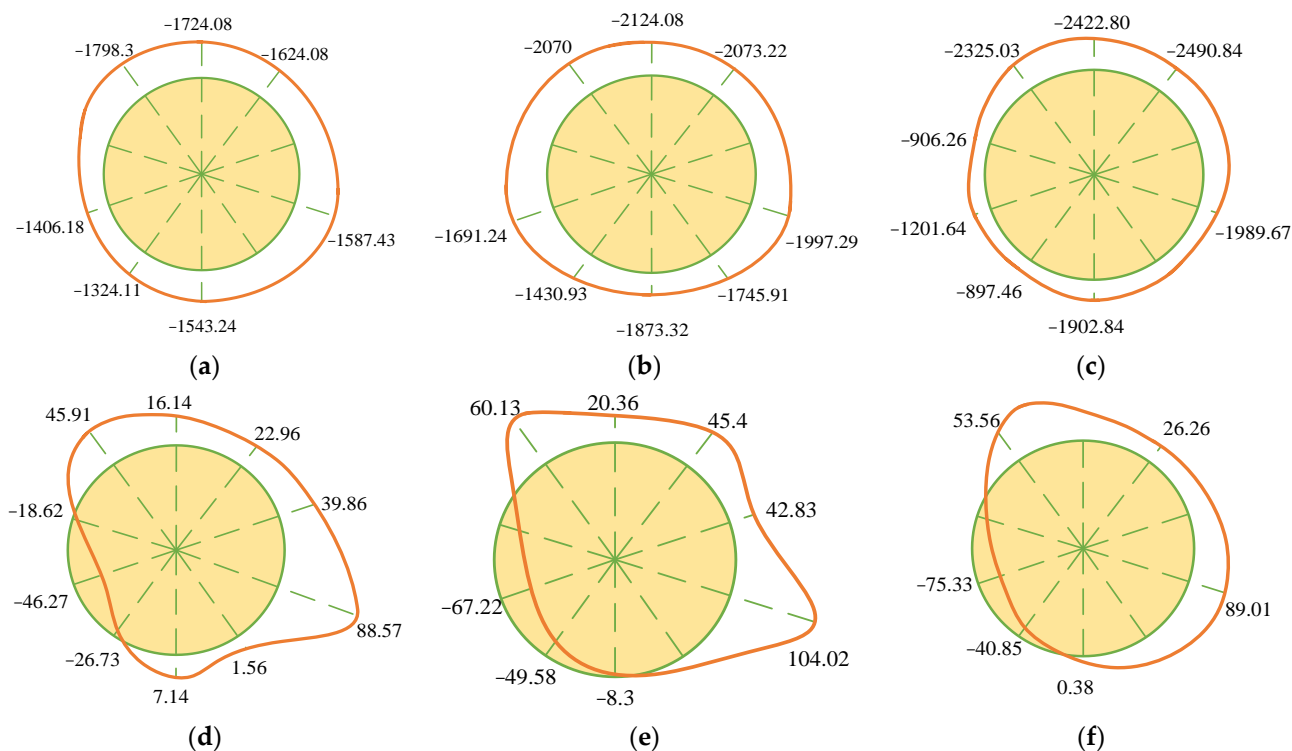


Figure 9. Segment internal force in soft and hard uneven formation: (a) Axial force (N) diagram of the segment when just spliced (kN). (b) The tube axis force (N) diagram when the shield tail comes out (kN). (c) Axial force (N) diagram of segment after stabilization (kN). (d) Bending moment (M) diagram of segment when newly spliced (kN·m). (e) Bending moment (M) diagram of shield tail pipe piece after escapement (kN·m). (f) Segment bending moment (M) diagram after stabilization (kN·m).

From Figure 9, it can be concluded that when the test ring segments are just assembled, because the segments are still protected by the shield shell, they are not affected by the formation pressure and grouting pressure. They are only affected by the segment's own weight and jack support. Because of the effect of the boots, the internal force of the test ring is small; when the segment comes out of the shield tail, the stress state of the segment changes. The synchronous grouting pressure, shield tail sealing brush and sealing grease pressure act on the outer surface of the segment. At the same time, the overlying formation pressure also passes through the grouting layer acting on the segment. At the time, the segment is in a complex three-dimensional stress state, and its internal force reaches the maximum value. Due to the need for shield attitude control, the jack needs to be adjusted at any time, which creates a pressure difference on the segment, which is very detrimental to the stress on the segment; when about 20 rings of the test ring segment are assembled, that is, on the fourth day after assembly at the beginning, since the slurry reaches 70% strength, the grouting pressure behind the shield tail basically no longer affects the test ring, and the internal force of the segment tends to be stable. The internal force of the segment after stabilization is generally smaller than when it just comes out of the shield tail. In strata with uneven softness and hardness, the ability of the soil to resist deformation is different, and the soil pressure on the left and right sides of the segment ring is not symmetrical.

4.1.3. Distribution Rules of Pore Water Pressure

In order to measure the pore water pressure more accurately and conveniently, after the test ring segment comes out of the No. 5 trolley of the shield machine, it is installed in the segment lifting hole. The water pressure change curve with construction and the layout of each measuring point are shown in Figures 10 and 11, respectively. As can be seen from the Figure 10, the 063# water pressure gauge at the arch waist reads 69.4 kPa after stabilization, and the 055# water pressure gauge at the bottom of the arch reads 94.9 kPa.

The difference between the two is 25.5 kPa, which is 15% different from the theoretically calculated 30 kPa; the 066# water pressure gauge at the arch waist reads 63.5 kPa after stabilization, and the 064# water pressure gauge at the bottom of the arch reads 89.5 kPa. The difference between the two is 26 kPa, which is 13.3% different from the theoretically calculated 30 kPa. This part of the gap may be due to the relatively complete slightly weathered rock layer near the arch bottom forming a water-proof layer that is not easily permeable, blocking the downward penetration of groundwater and causing hydraulic head loss.

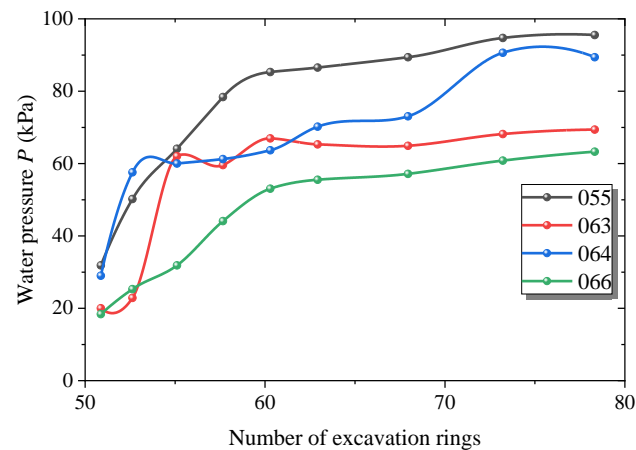


Figure 10. Pore water pressure (P) of each measuring point with construction.

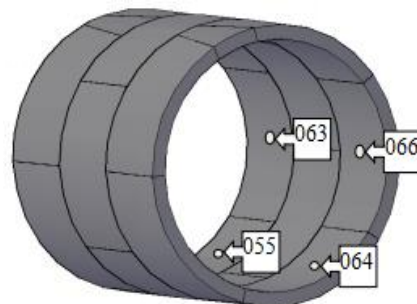


Figure 11. Arrangement of measuring point water pressure.

From this, we can derive the distribution law of pore water pressure in the shield segment in unevenly soft and hard strata: the size of groundwater pressure is related to hydraulic gradient, permeability coefficient, penetration velocity and penetration time. After the water pressure value is embedded in the segment lifting hole, the water pressure value at each measuring point gradually increases. In about two days, the pore water pressure value tends to be stable and basically remains unchanged. This is because the strongly weathered tuffaceous sandstone and weathered tuffaceous sandstone in this area have different strengths and hardnesses. The interfaces and even water passages between the strata are formed for the circulation of groundwater. The tuffaceous sandstone can pass through. There are also densely interconnected fissures distributed in the sandstone, which store part of the bedrock fissure water. Therefore, when groundwater is lost, the surrounding groundwater will continue to be replenished due to the hydraulic head difference until the hydraulic difference disappears and the water pressure reaches a stable equilibrium state. The softer rock layer in the upper part is a more permeable layer, and the groundwater pressure can be accurately reflected, but the harder rock layer in the lower part is equivalent to forming a water-proof layer that is not easily permeable, which will block the downward penetration of groundwater.

4.2. Clay Formation

4.2.1. Distribution Law of Soil Pressure on Pipe Segments

It can be seen from the soil pressure change curve with construction in Figure 12 that the soil pressure in clay strata changes during the construction process on the same principle as the change in soft and hard uneven strata, so the soil pressure after stabilization is shown in Figure 13.

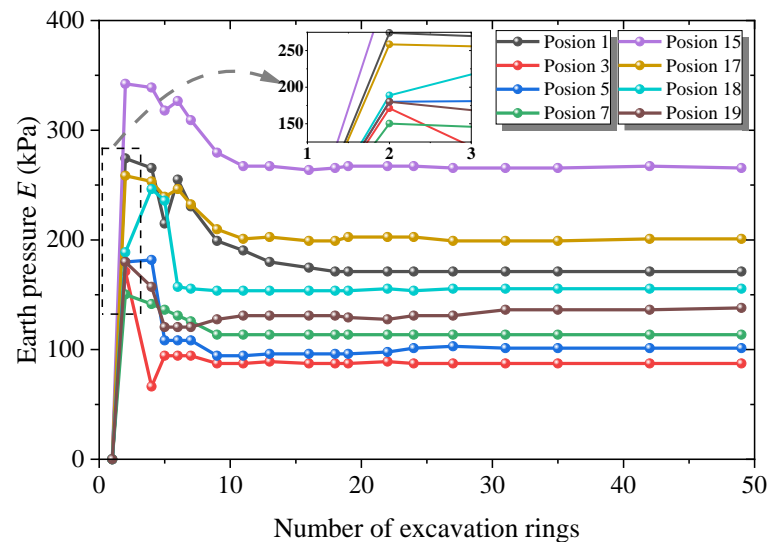


Figure 12. Earth pressure (E) with the construction changes.

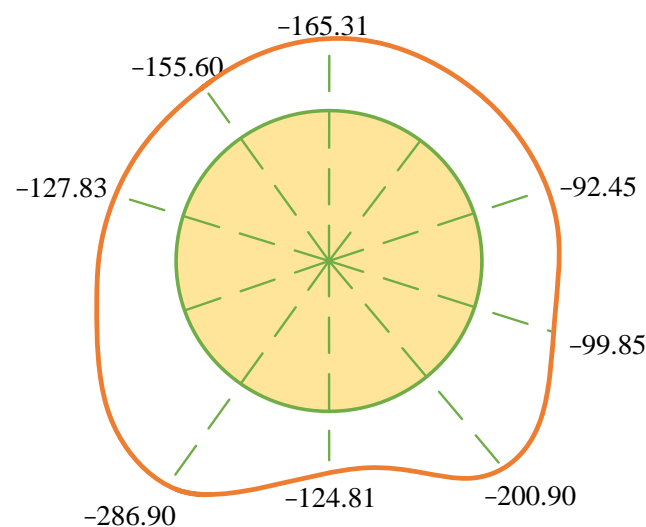


Figure 13. Arrangement of earth pressure (E) after stable (kPa).

Since the soil is gravelly clay soil with single properties and a low permeability coefficient, the simultaneous grouting effect is better, and the earth pressure distribution at each position of the test ring is relatively balanced. After the segment is stabilized, the vault is subject to vertical downward earth pressure, while the left and right sides of the segment are mainly subjected to horizontal earth pressure. Therefore, the earth pressure on the left and right sides is relatively small, but due to the influence of grouting pressure, the earth pressure at the left and right sides of the arch bottom close to the grouting hole is also relatively large, and the pressure at the top of the arch is much greater than the pressure at the bottom of the arch. During shield tunneling in gravelly clay soil strata, when the test ring segment breaks out of the shield tail ring 15, it will take about 3 to

4 days, and the stratum has basically reached a stable state. Due to the single geological conditions and consistent soil mechanical properties, after shield tunneling, the ground will complete settlement and deformation in a short period of time, forming an arch effect, thereby reaching a stable state.

4.2.2. Distribution Rules of Internal Forces in Segments

The variation curves of steel bar axial force with construction and concrete strain variation curves with construction are shown in Figures 14 and 15, respectively.

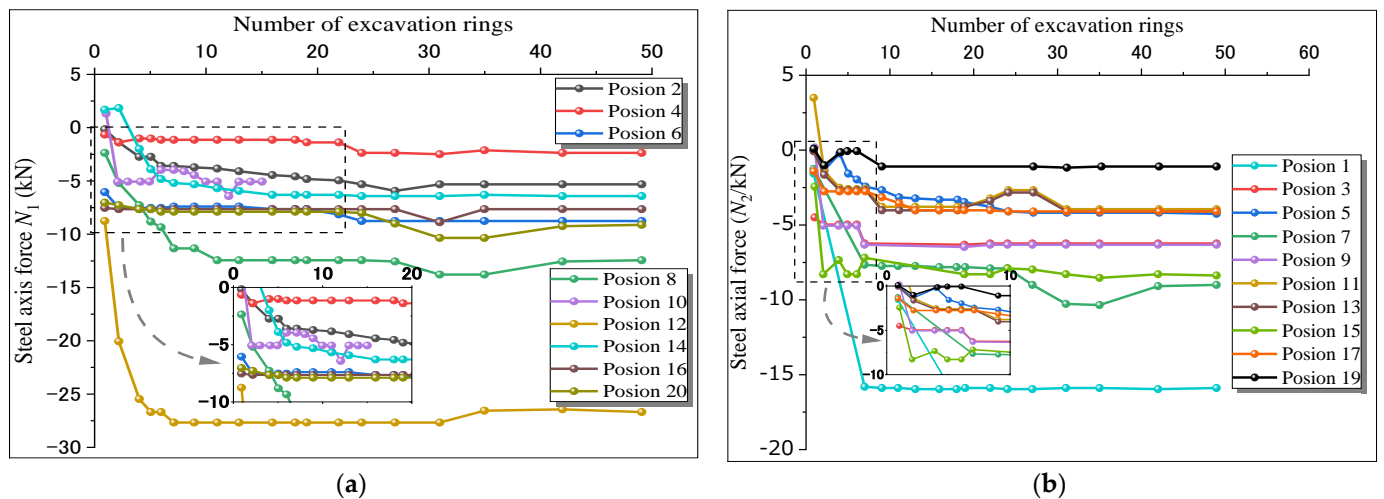


Figure 14. Steel axis force of each measuring point with the construction changes: (a) Axial force (N_1) change curve of inner steel bar. (b) Axial force (N_2) change curve of outer steel bars.

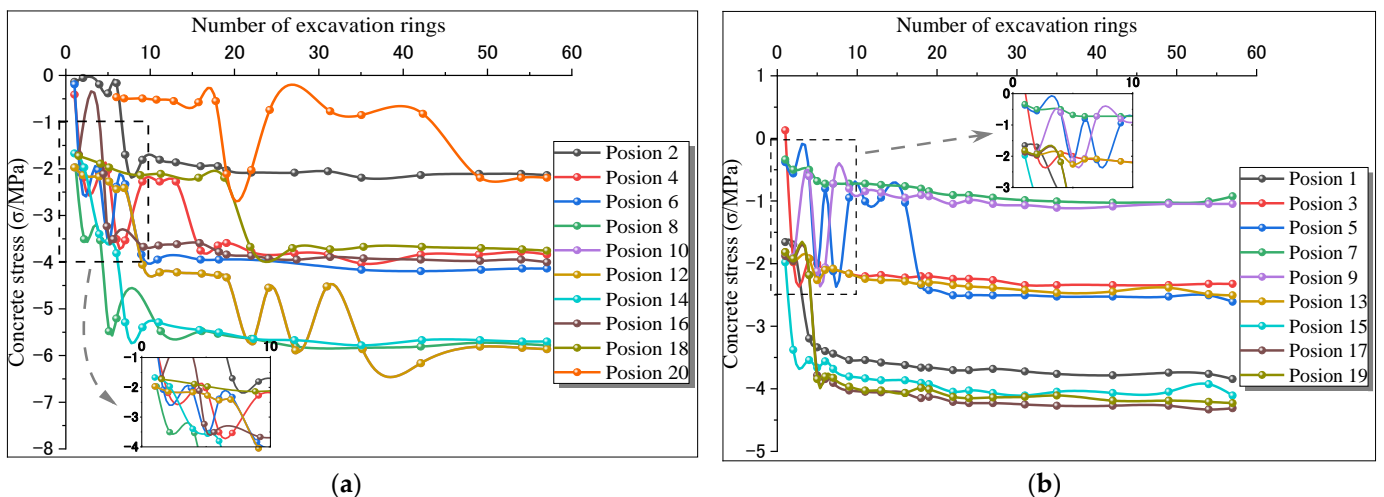


Figure 15. Concrete stress (σ) of each measuring point with the construction changes: (a) Inside concrete stress (σ) change curve. (b) External concrete stress (σ) change curve.

Based on the above-required internal forces of the steel bars and the internal forces of the concrete in each stage of the test ring, superimpose them to obtain the internal force distribution of the test ring segments in the three stages of just assembling, coming out of the shield tail and reaching stability, as shown in Figure 16.

It can be concluded from Figure 16 that the principle of internal force change in clay stratum segments is basically the same as that in unevenly soft and hard strata.

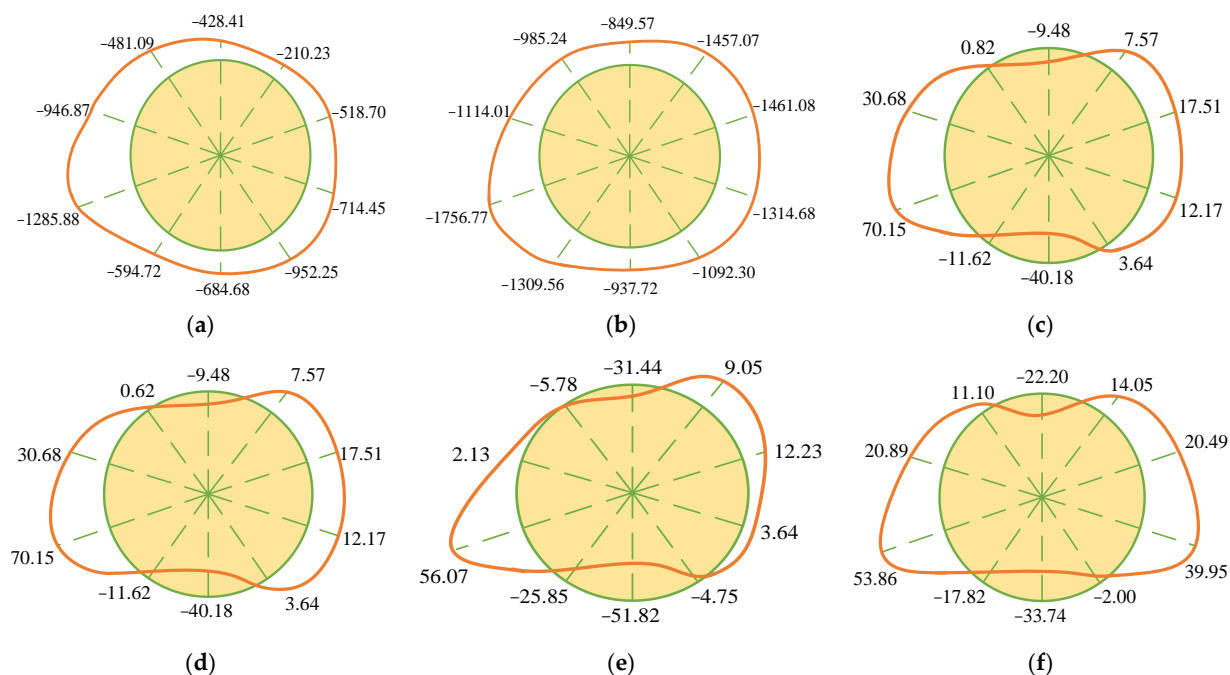


Figure 16. Segment internal force in clay ground: (a) Axial force (N) diagram of the segment when just spliced (kN). (b) The tube axis force (N) diagram when the shield tail comes out (kN). (c) Axial force (N) diagram of segment after stabilization (kN). (d) Bending moment (M) diagram of segment when newly spliced (kN·m). (e) Bending moment (M) diagram of shield tail pipe piece after escapement (kN·m). (f) Segment bending moment (M) diagram after stabilization (kN·m).

4.2.3. Distribution Law of Pore Water Pressure

The water pressure variation curve with construction and the layout of each measuring point are shown in Figures 17 and 18, respectively. As can be seen from the Figure 17, the 075# pore water pressure gauge is buried in the concrete at the bottom of the arch. The water pressure is 125 kPa, that is, there is a water head pressure of 12.5 m. This value is 45 kPa smaller than the actual 170 kPa water pressure, which is 26.5% smaller; at the same time, the 054# pore water pressure gauge is buried at the waist of the arch. Its burial depth is 19 m and the water pressure reaches 115 kPa. The difference in water pressure values between the two measuring points is only 10 kPa, which is 50% smaller than the actual 20 kPa water pressure difference. The main reason for the head loss is that the gravelly clay soil with a small permeability coefficient at the tunnel arch bottom partially blocks the flow of groundwater, resulting in the water pressure not being completely transmitted downward; at the same time, due to the blocking of the water pressure gauge and the segment grouting holes, the gaps between them are made of water-permeable cotton yarn, so some water pressure is lost.

From this, we can derive the distribution law of pore water pressure in the shield segment in clay strata: the size of groundwater pressure is related to hydraulic gradient, permeability coefficient, penetration velocity and penetration time. Because the clay particles are small, the pore water is mainly bound water, and water and soil particles are bonded together, making the pore water weakly permeable and unable to effectively transmit hydrostatic pressure. The recharge rate of groundwater is relatively slow, resulting in water pressure values at each measuring point. It takes about 60 h for the pore water pressure to rise slowly and stabilize, which is longer than the time required for the water pressure to stabilize in unevenly soft and hard formations. This is because the gravelly clay soil with a small permeability coefficient at the bottom of the tunnel arch fails to form an effective flow channel, blocking the flow of groundwater, and the water pressure cannot be completely transmitted downward, resulting in the actual water pressure at the bottom of the arch and the waist of the arch. The difference is smaller than the theoretical

difference. At the same time, groundwater pressure will be affected by rainfall. After rain, the groundwater level rises and the water pressure increases.

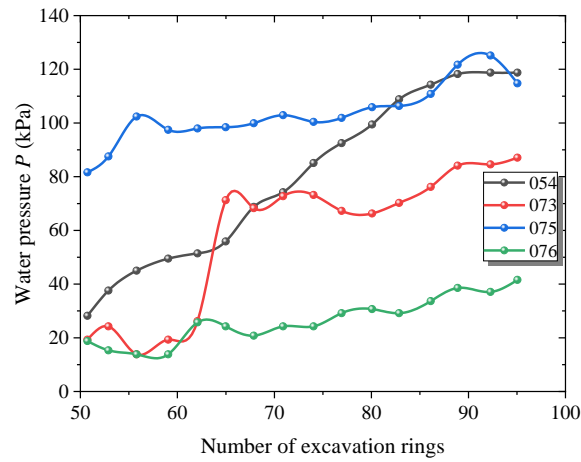


Figure 17. Pore water pressure (P) of each measuring point with construction.

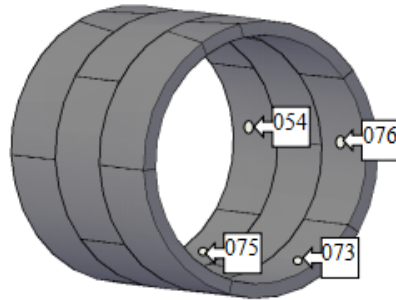


Figure 18. Arrangement of measuring point water pressure.

4.3. Proximity Pile Foundation

4.3.1. Distribution Law of Soil Pressure on Pipe Segments

It can be seen from the soil pressure change curve with construction in Figure 19 that the soil pressure of the adjacent pile foundation changes during the construction process on the same principle as the change of soft and hard uneven strata and clay strata. The stabilized soil pressure is shown in Figure 20.

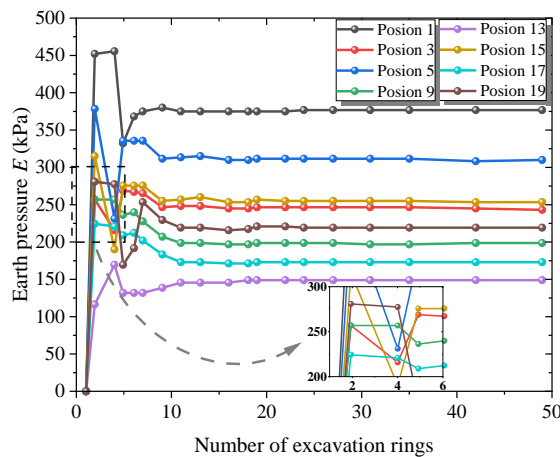


Figure 19. Earth pressure (E) with the construction changes.

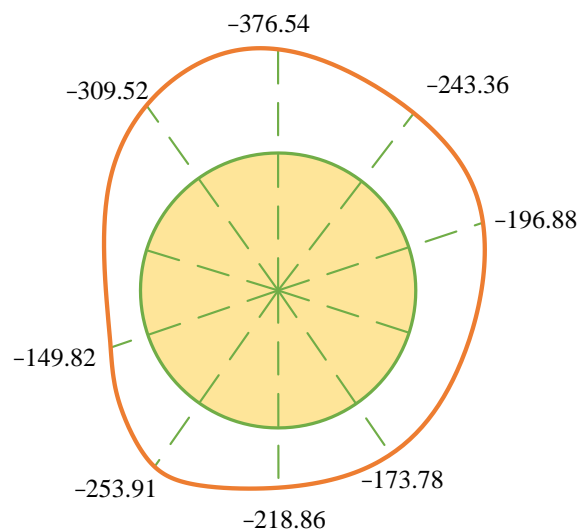


Figure 20. Arrangement of earth pressure (E) after stable (kPa).

Due to the large burial depth of the tunnel, which is nearly 20.5 m, the synchronous grouting effect is better and the earth pressure distribution at each position of the test ring is relatively balanced. The distance between the test ring vault and the building pile foundation is only 1.137 m. After the segment comes out of the shield tail, the load of the pile foundation will be transferred to the upper soil of the tunnel and finally to the lining segment. The vault is subject to a large vertical downward pressure, while the left and right sides of the segment are mainly subjected to horizontal earth pressure. Therefore, the earth pressure on the left and right sides is smaller than the earth pressure on the vault, but due to the influence of grouting pressure, the soil pressure near the four grouting holes is also relatively large, and the pressure on the vault is much greater than the pressure on the bottom of the vault. This also proves that the theory that the weight of the overlying soil is equal to the self-weight of the overlying soil on the vault is conservative when calculating the reaction force of the foundation at the bottom of the vault. In the shield tunneling construction close to the pile foundation, when the test ring segment breaks out of the 20 rings of the shield tail, the formation will basically reach a stable state in about 4 to 5 days. After the shield segment comes out of the shield tail, the ground building load is not transferred to the segment lining instantaneously but is a gradual process. While the building pile foundation undergoes a small amount of settlement deformation, most of the building load is gradually transferred. It is transferred to the segment until the arch balance effect is finally formed and the force balance state is reached.

4.3.2. Distribution Law of Internal Force in Pipe Segments

The variation curves of steel bar axial force with construction and concrete strain variation curves with construction are shown in Figures 21 and 22, respectively.

Based on the above-required internal forces of the steel bars and the internal forces of the concrete in each stage of the test ring, superimpose them to obtain the internal force distribution of the test ring segments in the three stages of just assembling, coming out of the shield tail and reaching stability, as shown in Figure 23.

It can be concluded from Figure 23 that the principle of internal force change in adjacent pile foundation segments is basically the same as that in uneven soft and hard strata and clay strata. However, due to the self-weight load of the building above the tunnel, the test ring segment was subject to greater additional stress. The internal force of the segment was much greater than that without the overlying building. It also proved that the reinforced special shield ring was used here. The design of the segment is reasonable.

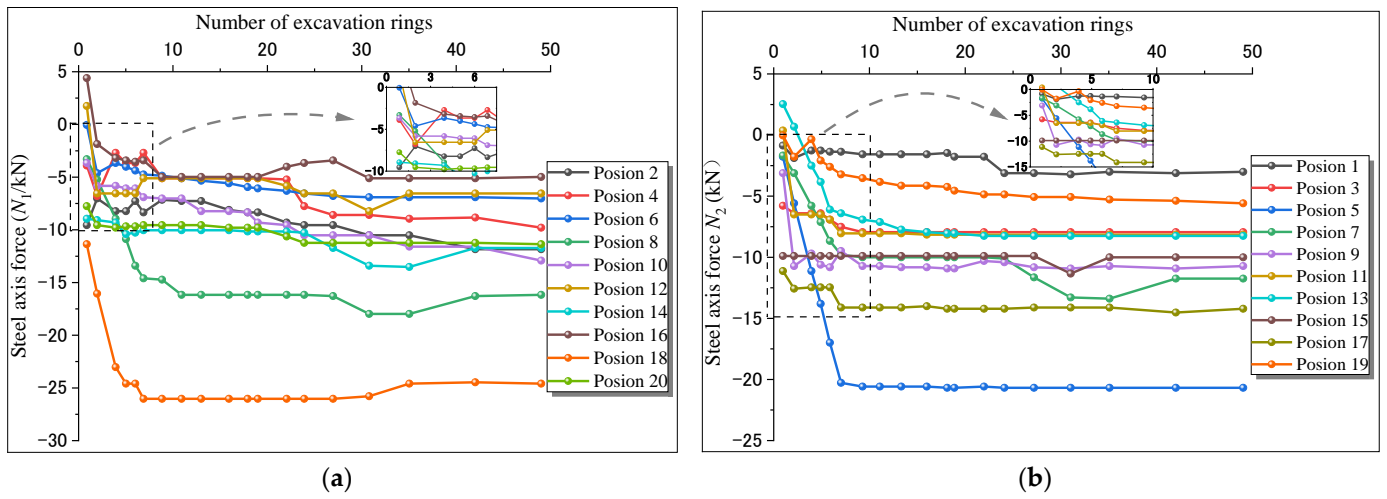


Figure 21. Steel axis force of each measuring point with the construction changes: (a) Axial force (N_1) change curve of inner steel bar. (b) Axial force (N_2) change curve of outer steel bars.

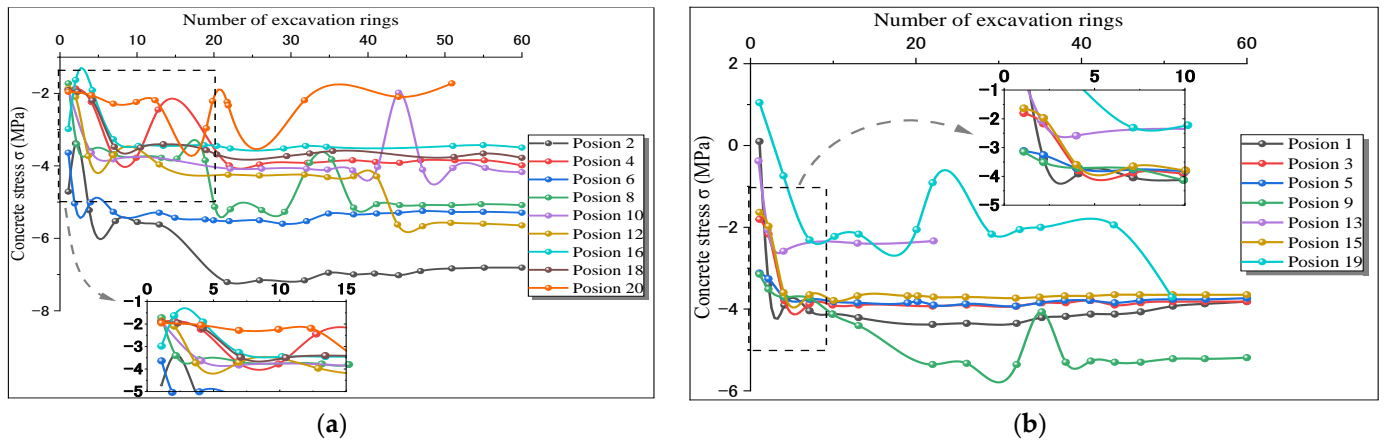


Figure 22. Concrete stress (σ) of each measuring point with the construction changes: (a) Inside concrete stress (σ) change curve. (b) External concrete stress (σ) change curve.

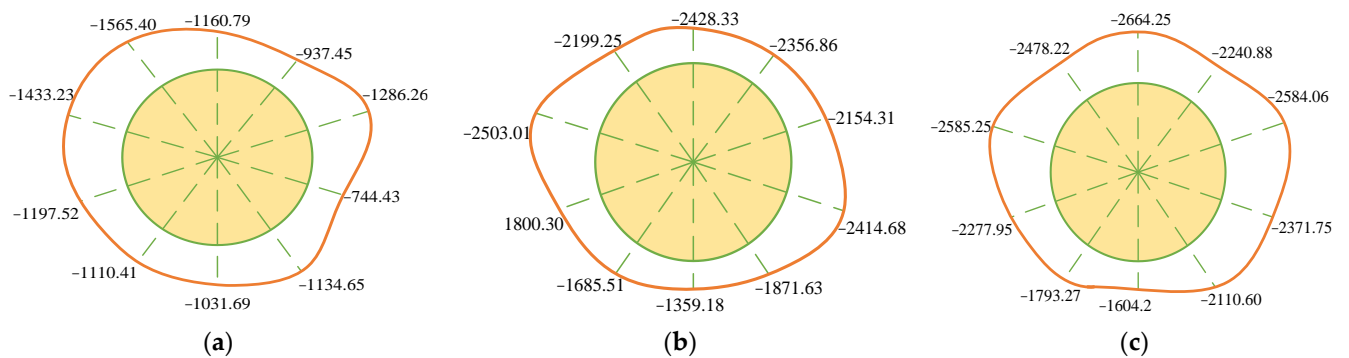


Figure 23. Cont.

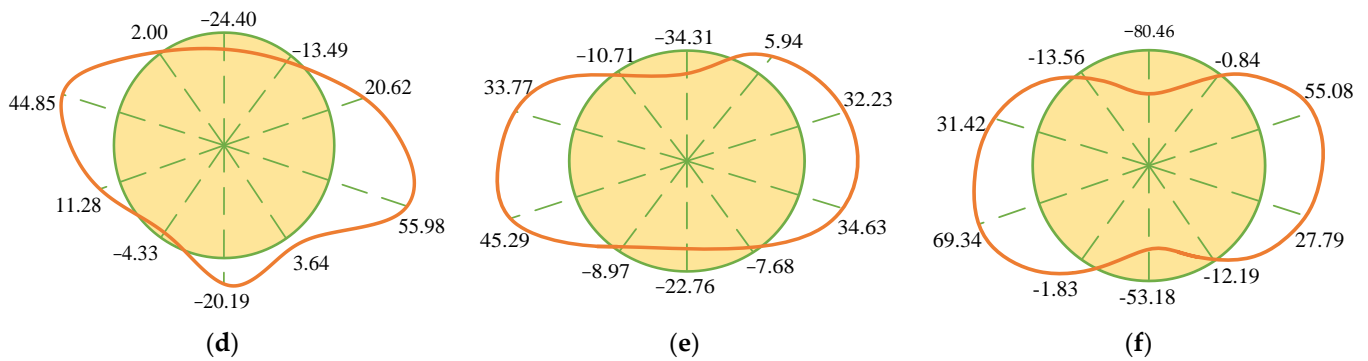


Figure 23. Segment internal force in proximity pile foundation: (a) Axial force (N) diagram of the segment when just spliced (kN). (b) The tube axis force (N) diagram when the shield tail comes out (kN). (c) Axial force (N) diagram of segment after stabilization (kN). (d) Bending moment (M) diagram of segment when newly spliced (kN·m). (e) Bending moment (M) diagram of shield tail pipe piece after escapement (kN·m). (f) Segment bending moment (M) diagram after stabilization (kN·m).

4.3.3. Distribution Law of Pore Water Pressure

The water pressure variation curve with construction and the layout of each measuring point are shown in Figures 24 and 25, respectively. It can be seen from the water pressure distribution curve that the 072# pore water pressure meter is buried in the concrete on the right side of the arch bottom. The water pressure at the bottom of the arch is 210 kPa and has a head pressure of 21 m. This water pressure value is very close to the theoretical value. This is because the rock formation is relatively fragmented, with a large number of water passages and fissures, and the groundwater pressure value can be accurately reflected by the pore water pressure. At the same time, double-fast cement is used to seal the gap between the water pressure gauge and the segment grouting hole, which can completely seal the gap between the lifting hole and the water pressure gauge. The specific method is as follows: before adding double-fast cement into the gap, first insert a thin plastic pipe to allow water to flow out from behind the lifting hole, so as not to affect the consolidation of the double-fast cement. After the cement is completely solidified the next day, tie the plastic pipe tightly with a tie wire to completely block the water flow in the grouting hole. This method has a very good blocking effect. The water pressure reaches stability quickly and there is almost no water head loss, which reflects the real water pressure.

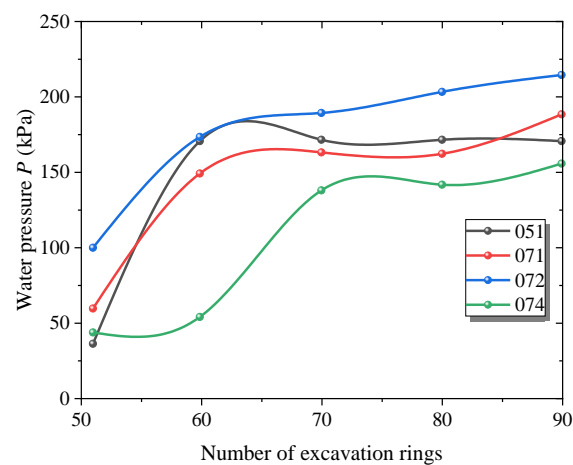


Figure 24. Pore water pressure (P) of each measuring point with construction.

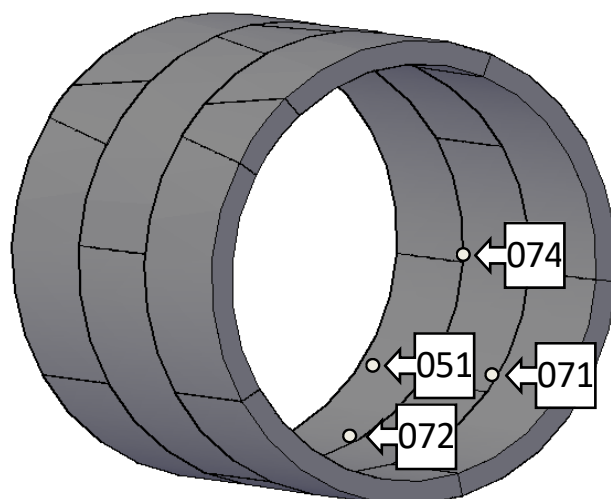


Figure 25. Arrangement of measuring point water pressure.

From this, it can be concluded that the distribution law of pore water pressure in the shield segment when close to the pile foundation is as follows: the size of groundwater pressure is related to hydraulic gradient, permeability coefficient, penetration velocity and penetration time. The water pressure value at each measuring point rises rapidly, and the water pressure value tends to be stable 24 h after the pore water pressure gauge is installed. This is because the test ring is located in a fully weathered and strongly weathered granite layer. The rock layer is relatively broken and extremely developed. There are many groundwater occurrence zones in the rock layer, which can store a large amount of bedrock fissure water and loose rock pore water. At the same time, the rock layers have formed an interface for groundwater to flow. Therefore, when groundwater is lost, groundwater in other locations can be replenished at a faster rate until the hydraulic pressure difference disappears and a hydraulic equilibrium state is finally reached. The burial depth of this section is relatively large. At the same time, it is not far from the location of the preset water collection tank, only about 100 m. It is the lower point of the tunnel. Groundwater in the entire tunnel will accumulate here, which will also cause the water pressure of this section to increase.

5. Conclusions

Through field tests to ascertain the mechanical properties of shield tunnel segments in complex strata in Shenzhen, the following conclusions can be drawn:

- (1) In the stratum with uneven hardness, the hardness of soil varies, the earth pressure on the left and right sides of the test ring is asymmetric, and the vault pressure is greater than the arch bottom pressure. There are water passages and bedrock fissure water in the stratum, and the surrounding groundwater will continuously replenish the groundwater loss here because of the head difference until the water pressure reaches a stable equilibrium state; in clay stratum, the soil is gravelly cohesive soil with a single property and low permeability coefficient, and the earth pressure distribution at each position of the segment ring is relatively balanced. There is no effective flow channel in the gravel cohesive soil layer, and the water pressure can not be completely transmitted downwards, which leads to the actual water pressure difference between the arch bottom and the arch waist being smaller than the theoretical difference; in the fully weathered granite layer of the overlying building, the segment of the test ring is subjected to greater additional stress, which is much greater than the internal force of the segment without the overlying building. A boundary surface for groundwater circulation is formed between rock strata, which can store a large amount of fissure water and pore water. Groundwater in other places can supply groundwater loss here at a faster speed, and finally reach a state of hydraulic balance.

- (2) The mechanical properties of shield tunnel segments in different strata are quite different, but their mechanical properties change stages are consistent. That is, when the segment ring is just assembled, under the protection of the shield shell, the internal force is small, and when the segment comes out of the shield tail, the internal force of the segment reaches the maximum peak. When the segment is assembled for a certain period of time, the internal force of the segment tends to be stable, and the internal force of the stabilized segment is generally smaller than when it just comes out of the shield tail.

The calculation method and practical problems based on the rectangular model used in this paper involve many theories, methods and technologies. There are still many new problems to be solved in this paper, which need to be accumulated and improved in practical application. Further research is needed in the following aspects. In the analysis of uneven soft and hard strata, this paper only considers the mechanical characteristics of segments in the upper soft and lower hard strata, but does not consider the upper hard and lower soft strata. These strata can be further distinguished to increase the integrity of the content; this paper only considers some basic force analysis of the pipe segment and does not conduct more in-depth research on other important characteristics of the pipe segment.

Author Contributions: H.H. proposed the research plan and framework ideas for this article and completed the writing—original draft; T.X. provided financial support for the research of the project and investigated the geological conditions and distribution of buildings and structures within the study area; J.L. provided the mechanical performance parameters of the segment material and the internal reinforcement configuration, and provided assistance for embedding sensors and other testing components in the production process of shield segments; P.L. provided detailed geological parameters, shield tunnel and segment structural size data, as well as shield tunneling parameters and other information for this study; B.W. processed the data collected from on-site shield tunneling segments and optimized the readability of the charts. Y.L. optimized the organizational structure of the article and offered useful suggestions for the preparation and writing of the paper. All authors have read and agreed to the published version of the manuscript.

Funding: This study was supported by the National Natural Science Foundation of China (NSFC) under Grant No. 51508037.

Data Availability Statement: Data are contained within the article.

Acknowledgments: We highly appreciate the data collection and processing work of China Railway Eryuan Engineering Group Co., Ltd. China Railway Materials Group Xinjiang Co., Ltd. Finally, the authors would like to thank the reviewers for their useful comments and the editors for improving the manuscript.

Conflicts of Interest: Author Tao Xue was employed by the company China Communications Construction Company Limited; Author Jianjun Li was employed by the company China Railway Materials Group Xinjiang Co., Ltd.; Author Peisi Liu was employed by the company China Railway Eryuan Engineering Group Co., Ltd. The remaining authors declare that the research was conducted in the absence of any commercial or financial relationships that could be construed as a potential conflict of interest.

References

1. Qin, B.Y.; Li, H.Y.; Wang, Z.J.; Jiang, Y.; Lu, D.C.; Du, X.; Qian, Q.L. New Framework of Low-Carbon City Development of China: Underground Space Based Integrated Energy Systems. *Undergr. Space* **2024**, *14*, 300–318. [[CrossRef](#)]
2. Zhang, H.; Chen, L.; Zhu, Y.M.; Zhou, Z.L.; Chen, S.G. Stress Field Distribution and Deformation Law of Large Deformation Tunnel Excavation in Soft Rock Mass. *Appl. Sci.* **2019**, *9*, 865. [[CrossRef](#)]
3. Zhu, Y.M.; Chen, L.; Zhang, H.; Zhou, Z.L.; Chen, S.G. Physical and Mechanical Characteristics of Soft Rock Tunnel and the Effect of Excavation on Supporting Structure. *Appl. Sci.* **2019**, *9*, 1517. [[CrossRef](#)]
4. Zeng, Y.H.; Liu, K.L.; Fang, Y.; Zhang, X.F.; Bai, Y. Fire Model Test on Temperature Field in the Rescue Station of an Extralong Railway Tunnel. *Adv. Civ. Eng.* **2019**, *2019*, e1732572. [[CrossRef](#)]
5. Zhang, H.; Chen, L.; Chen, S.G.; Sun, J.C.; Yang, J.S. The Spatiotemporal Distribution Law of Microseismic Events and Rockburst Characteristics of the Deeply Buried Tunnel Group. *Energies* **2018**, *11*, 3257. [[CrossRef](#)]

6. Zhang, S.F.; Gao, Z.H.; Wang, S.; Chen, B.; Mao, C.Z. Study on the Seismic Response Characteristics of Shield Tunnels with Different General Segment Assembly Methods and Widths. *Buildings* **2023**, *13*, 2039. [\[CrossRef\]](#)
7. Xu, X.D.; He, M.C.; Zhu, C.; Lin, Y.; Cao, C. A New Calculation Model of Blasting Damage Degree—Based on Fractal and Tie Rod Damage Theory. *Eng. Fract. Mech.* **2019**, *220*, 106619. [\[CrossRef\]](#)
8. Sazid, M.; Singh, T.N. Two-Dimensional Dynamic Finite Element Simulation of Rock Blasting. *Arab J. Geosci.* **2013**, *6*, 3703–3708. [\[CrossRef\]](#)
9. Sazid, M. Effect of Underground Blasting on Surface Slope Stability: A Numerical Approach. *Am. J. Min. Metall.* **2017**, *4*, 32–36.
10. Lin, F.; Zhang, H.; Chen, S.G. Study on Type Selection of Shield Equipment in Different Geological Conditions. In *Green Building, Materials and Civil Engineering*; CRC Press: Boca Raton, FL, USA, 2014; ISBN 978-0-429-22702-8.
11. Zou, J.F.; Qian, Z.H.; Xiang, X.H.; Chen, G.H. Face Stability of a Tunnel Excavated in Saturated Nonhomogeneous Soils. *Tunn. Undergr. Space Technol.* **2019**, *83*, 1–17. [\[CrossRef\]](#)
12. Zhang, H.; Chen, S.G.; Deng, X.F. Analysis of the influence of shield driving parameters on ground settlements. *Mod. Tunn. Technol.* **2010**, *47*, 48–53.
13. Liao, S.M.; Liu, J.H.; Wang, R.L.; Li, Z.M. Shield Tunneling and Environment Protection in Shanghai Soft Ground. *Tunn. Undergr. Space Technol.* **2009**, *24*, 454–465. [\[CrossRef\]](#)
14. Zhang, J.L.; Gao, Y.M.; Liu, X.; Zhang, Z.A.; Yuan, Y.; Mang, H.A. A Shield Tunneling Method for Enlarging the Diameter of Existing Tunnels: Experimental Investigations. *Tunn. Undergr. Space Technol.* **2022**, *128*, 104605. [\[CrossRef\]](#)
15. Xie, X.Y.; Yang, Y.B.; Ji, M. Analysis of Ground Surface Settlement Induced by the Construction of a Large-Diameter Shield-Driven Tunnel in Shanghai, China. *Tunn. Undergr. Space Technol.* **2016**, *51*, 120–132. [\[CrossRef\]](#)
16. Zhang, H.; Chen, S.G.; Tan, X.R. Research on the mechanical behavior of a segment of a shield tunnel adjacent to a pile foundation. *Mod. Tunn. Technol.* **2012**, *49*, 101–107.
17. Zhang, H.; Chen, S.G.; Deng, X.F. Analysis on influence of shield tunneling on ground and bridge pile. *Tunn. Undergr. Space Technol.* **2011**, *7*, 552–557.
18. Xu, Z.W.; Zhou, S.H.; Zhang, C.; Yang, M.H.; Jiang, M.Y. A Bayesian Network Model for Suitability Evaluation of Underground Space Development in Urban Areas: The Case of Changsha, China. *J. Clean. Prod.* **2023**, *418*, 138135. [\[CrossRef\]](#)
19. Yan, Z.G.; Li, J.T.; Shen, Y.; Xiao, Z.Q.; Ai, Q.; Zhu, H.H. Damage Identification Method on Shield Tunnel Based on PLSR and Equivalent Damage Analysis. *Tunn. Undergr. Space Technol.* **2023**, *137*, 105127. [\[CrossRef\]](#)
20. Sazid, M.; Hussein, K.; Abudurman, K. Rock Stress Measurement Methods in Rock Mechanics—A Brief Overview. *World J. Eng. Technol.* **2023**, *11*, 252–272. [\[CrossRef\]](#)
21. Zhu, W.B.; Ju, S.J. *Shield Tunneling Technology in Mixed Face Ground Conditions*; China Science and Technology Press: Beijing, China, 2006; ISBN 978-7-5046-4327-8.
22. Fang, Y.; Fu, Y.P.; Qi, C.; He, C. Structural load and internal force characteristics of shield tunnel segment in expansive rock and soil strata. *China Railw. Sci.* **2014**, *35*, 56–63.
23. Zhang, H.; Chen, S.G.; Tan, X.R.; Zhao, Y.B. Research on Mechanical Behaviour of Segmental Structure of Shield Tunnel in Different Strata. *Chin. J. Undergr. Space Eng.* **2015**, *11*, 845–851.
24. Zhang, X.H.; Zhou, S.H.; Di, H.G.; Wang, P.X.; Wang, J.T. Semi-Analytical Solution for Ultimate Bearing Capacity of Straight-Jointed Segmental Tunnel Lining. *Tunn. Undergr. Space Technol.* **2023**, *138*, 105160.
25. Song, K.Z.; Yuan, D.J.; Wang, M.S. Segmental mechanical analysis of shield tunnel during construction stage. *Rock Soil Mech.* **2008**, *29*, 619–623+628.
26. Huang, D.W.; Jiang, H.; Xu, C.J.; Li, X.; Zhan, T. Analytical Algorithm of Longitudinal Bending Stiffness of Shield Tunnel Considering Longitudinal Residual Jacking Force. *Tunn. Undergr. Space Technol.* **2023**, *137*, 105146. [\[CrossRef\]](#)
27. Liu, Y.B.; Liao, S.M.; Liu, M.B.; Chen, L.S. A Bending-Shear-Torsion Resistant Beam Foundation Model for Segmental Tunnels in Longitudinal Direction. *Tunn. Undergr. Space Technol.* **2023**, *140*, 105296. [\[CrossRef\]](#)
28. Chen, J.S.; Mo, H.H. Three-dimensional finite element analysis of mechanical behaviors of shield tunnel segment during construction. *Chin. J. Rock Mech. Eng.* **2006**, *25*, 3482–3489.
29. Zhu, W.B.; Ju, S.J. Causes and countermeasures for segment cracking in shield-driven tunnel. *Mod. Tunn. Technol.* **2003**, *40*, 21–25. [\[CrossRef\]](#)
30. Zhu, H.H.; Cui, M.Y.; Yang, J.S. Design model for shield lining segments and distribution of load. *Chin. J. Geotech. Eng.* **2000**, *22*, 190–194.
31. Zhu, H.H.; Tao, L.B. Study on two beam-spring models for the numerical analysis of segments in shield tunnel. *Rock Soil Mech.* **1998**, *19*, 26–32.
32. Chen, W.; Peng, Z.B.; Tang, M.X. Testing study on work property of shield segment. *Chin. J. Rock Mech. Eng.* **2004**, *23*, 959–963.
33. Hu, Z.P.; Luo, L.J.; Cai, Z.Y. Study on flatshell-elastic hinge-foundation model in shield tunnel. *Rock Soil Mech.* **2005**, *26*, 1403–1408.
34. Kong, X.X.; Tang, L.; Ling, X.Z.; Li, H. Development of Shield Model Test System for Studying the Bias Load of Shield in Soil-Rock Compound Strata. *Tunn. Undergr. Space Technol.* **2024**, *143*, 105464. [\[CrossRef\]](#)
35. Zhu, Y.T.; Zhu, Y.F.; Chen, E.J.; Zhai, Y.X.; Min, R.; Tang, B.; Huang, X. Synchronous Shield Tunnelling Technology Combining Advancement and Segment Fabrication: Principle, Verification and Application. *Undergr. Space* **2023**, *13*, 23–47. [\[CrossRef\]](#)
36. Sazid, M.; Ahmed, H.A. Stability Analysis of Shallow Depth Tunnel in Weak Rock Mass: 3D Numerical Modeling Approach. *J. City Dev.* **2019**, *1*, 18–22.

-
37. Verma, A.K.; Singh, T.N. Assessment of Tunnel Instability—A Numerical Approach. *Arab. J. Geosci.* **2010**, *3*, 181–192. [[CrossRef](#)]
 38. *GB 50010-2010*; Code for Design of Concrete Structures. China Building Industry Press: Beijing, China, 2015.

Disclaimer/Publisher’s Note: The statements, opinions and data contained in all publications are solely those of the individual author(s) and contributor(s) and not of MDPI and/or the editor(s). MDPI and/or the editor(s) disclaim responsibility for any injury to people or property resulting from any ideas, methods, instructions or products referred to in the content.